Shock melting of cerium

B. J. Jensen,* F. J. Cherne, and J. C. Cooley
Los Alamos National Laboratory, Los Alamos, New Mexico 87545, USA

M. V. Zhernokletov and A. E. Kovalev
RFNC-VNIIEF, Sarov, Nizhni Novgorod Region 607190, Russia

(Received 2 April 2010; revised manuscript received 21 May 2010; published 14 June 2010)

Shock-wave experiments were performed to examine the melt transition for cerium. Despite past work which points to a higher-pressure transition, the large volume collapse associated with the low-pressure γ-α phase transition is expected to result in a low-pressure melt transition. Multiple experimental configurations including front-surface impact and transmission experiments using velocimetry were used to obtain Hugoniot data and sound-speed data for impact stresses up to approximately 18 GPa. Sound-speed data exhibit a structured release consisting of a longitudinal wave followed by a slower plastic wave. The difference between these two wave speeds is observed to decrease with increasing impact stress until a single shock wave is observed indicating the onset of the melt transition which was estimated to be 10.24 ± 0.34 GPa. Additional data show that the sound speed is in agreement with liquid data at approximately 18 GPa likely indicating the completion of the melt transition. Further results and implications are discussed.

DOI: 10.1103/PhysRevB.81.214109 PACS number(s): 62.50.Ef, 64.70.dj

I. INTRODUCTION

Shock-wave experiments examining phase transitions in materials have been of general interest for more than half a century[1] with considerable emphasis on shock-induced melting of metals.[2–9] Unlike many metals which melt at relatively high temperatures and pressures, cerium metal is expected to exhibit a low-pressure melt transition for shock wave loading due to the large volume collapse associated with the γ-α transition.[10–12] In addition, cerium exhibits a rich phase diagram[13] (see Fig. 1) with four solid phases at zero pressure, at least three more phases at higher pressure,[14–16] and an anomalous melt boundary.[17,18] This rich phase diagram exists at relatively moderate stresses which are readily accessible using standard shock-wave methods making cerium an ideal material for studies focused on the multiphase equation-of-state and strength properties of materials.[19]

Past work on cerium has shown that the low-pressure shock response is anomalous in the γ phase and undergoes a 13–16 vol % collapse as it transforms to the α phase.[20] The anomalous behavior followed by the volume collapse leads to a structured wave profile that consists of a ramp wave followed by a shock wave (see Fig. 1 inset).[21] With increasing pressure, the ramp wave is easily overdriven leading to a single shock wave that propagates through the sample. The high-pressure response of cerium was initially examined by Carter[22] using explosive shock-wave methods to reach impact stresses up to 140 GPa. Breaks in the shock velocity data at 10 and 48 GPa were interpreted as a low-pressure solid-solid transition followed by a higher-pressure melt transition, respectively. Subsequent work by Zhernokletov[23] found good agreement with the Hugoniot data but the sound-speed data did not show a high-pressure melt transition. More recently, theoretical progress has been made for cerium which included the development of a complete multiphase equation-of-state[24] that focused on the well-known γ-α phase transition. This model predicted a melt transition of 11.3 GPa (at $T=1130$ K) for shock compression. Despite the efforts to obtain static data and high-pressure dynamic data for cerium, the dynamic melt transition for shock compression has not been established experimentally.

The main objective of the current work was to examine the dynamic melt transition for cerium by performing shock-

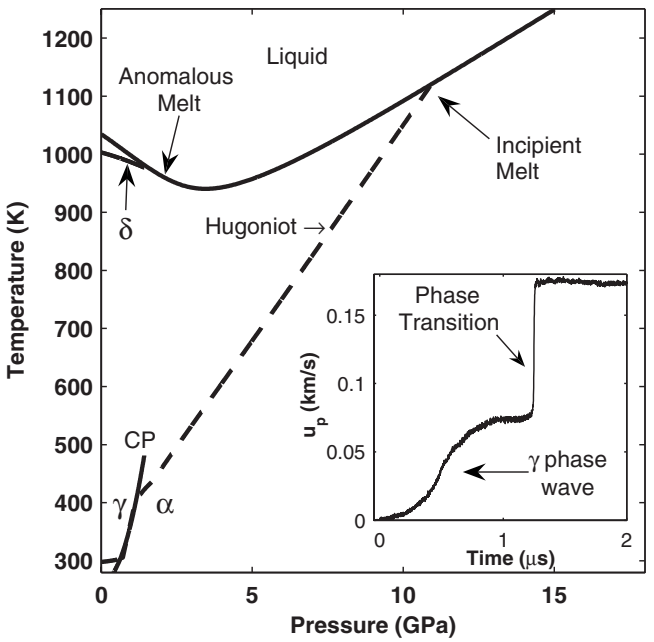

FIG. 1. Partial phase diagram for cerium showing multiple phases at low pressures. The melt boundary, γ-α boundary and the Hugoniot curve (or shock adiabat) were obtained from a multiphase EOS that was based on available static data (Ref. 13). The δ-phase boundary (Ref. 12) and solid-solid critical point are also indicated. (Inset) Example of shock-wave data (particle velocity vs time) showing the structured wave for cerium samples shocked to stresses in the vicinity of the γ-α phase transition. The large-volume collapse at the γ-α phase boundary is expected to result in a low-pressure melt transition.

wave experiments to determine the solid and liquid Hugoniots and sound speeds as a function of pressure. Velocity Interferometer System for Any Reflector (VISAR) and photonic Doppler velocimetry (PDV) were used to measure the shock-wave profile, to obtain Hugoniot data, and the sound speeds for impact stresses up to approximately 18 GPa that are expected to span the melt transition. These data coupled with additional cerium data reported elsewhere[22,23] were used to define the solid and liquid Hugoniots for cerium and estimate the melt transition stress.

The experimental methods are discussed in Sec. II followed by the experimental results in Sec. III. The data are analyzed in Sec. IV followed by summary and conclusions in Sec. V.

II. EXPERIMENTAL METHODS

As compared to other pressure-induced phase transitions such as the α-ϵ transition for iron,[25,26] the signature for the melt transition can often be more subtle because the density- and wave-speed differences are too small to be seen in wave-profile data.[2] In contrast, sound-speed measurements are more sensitive to changes in the material properties and have proven useful for detecting phase transitions including melt.[2,5] The standard experimental configuration for measuring sound speeds at pressure is the overtake method[27,28] which uses multiple samples (of varying thickness) to monitor the release wave as it overtakes the shock wave. Another experimental method that can provide sound-speed data (with increased uncertainty in the Hugoniot data) is the front-surface (F) impact configuration[26,29] where the sample impacts the optical window and the particle velocity history at the impact surface is measured. Both methods were used in this work to obtain Hugoniot and sound-speed data to identify the melt transition for cerium.

Plate impact experiments were performed using multiple gun facilities including a low-velocity 50-mm bore gas gun (0.1–0.8 km/s), a high performance 40-mm powder gun (0.1–2 km/s), and a 90-mm bore powder gun[30,31] (0.1–2.3 km/s). The experimental configuration for front-surface impact experiments is shown in Fig. 2 which consisted of a cerium sample backed by syntactic foam impacting a LiF optical window front plated with aluminum. Accurate particle velocity histories were obtained at the cerium-LiF interface near the center of the sample using VISAR (Ref. 32) and PDV.[33] These data coupled with the measured projectile velocity and the known shock response of the optical window were used to determine the Hugoniot state for cerium[26] and the sound speed at pressure.

The experimental configuration for transmission (T) experiments is also shown in Fig. 2 which consisted of an impactor (backed by syntactic foam) and a baseplate (same material as the impactor) backed by the cerium sample and optical window assembly. One VISAR probe was located on the sample center to obtain the particle velocity history at the cerium-LiF interface. Three PDV probes were placed about the sample to monitor shock arrival at the front of the cerium sample and at the cerium-LiF interface to determine the shock velocity, shock wave tilt, and to obtain additional particle velocity data. The Hugoniot state was determined using the standard impedance matching method.[34] Some transmission experiments were performed on a large-bore powder gun[30] which used four cerium samples (per target) of varying thickness (1–5 mm) to determine the sound speed at pressure using the overtake method.[27,28] For all experimental configurations, piezoelectric impact pins were used to measure impact tilt and to provide diagnostic trigger signals. Projectile velocities were measured using either the standard shorting pin method or Doppler velocimetry.[33]

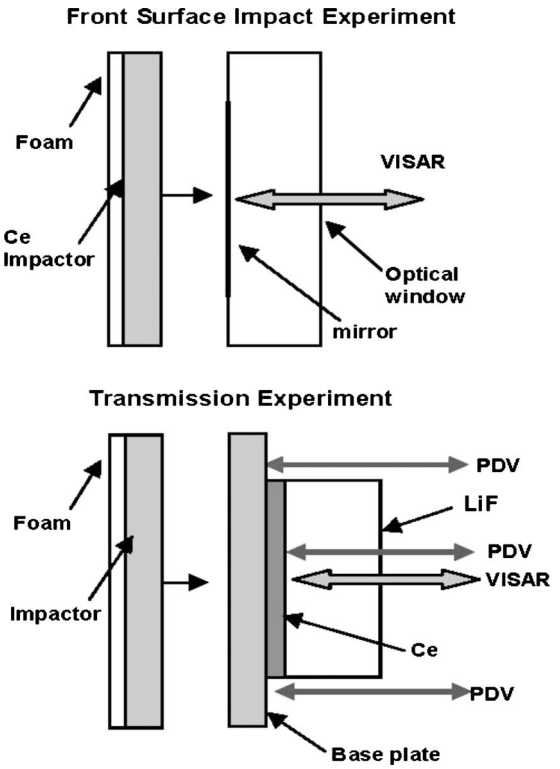

FIG. 2. Schematic of the front-surface and transmission experimental configurations used in this work. Approximate locations of the VISAR and PDV probes are indicated. Impactor and base plate materials are shown in Table I (column 2).

The PDV and VISAR systems used in this work along with the data analysis have been discussed in detail elsewhere.[33] For the PDV system, 1550-nm laser light was transmitted to and from the target using standard SMF-28 optical fiber and either collimated probes (Lightpath or AC photonics grin probes) or Oz-optics focusing probes (21-mm or 48-mm focal lengths). Because the PDV system can resolve multiple velocities simultaneously, some of the PDV probes used on the multislug experiments were multiplexed together (baseplate-sample pairs) using AC-photonics 50-50 splitters to minimize the number of digitizer channels required for the experiment. Base plate materials included 6061-T6 aluminum,[35] OFHC copper,[5] and 304 stainless steel.[36] All experiments used high-purity (99.99%) cerium samples[37] produced by MST (LANL) with a measured initial density 6.687 ± 0.038 g/cc, an ambient longitudinal sound speed of 2.339 ± 0.020 km/s, a shear-wave speed of 1.326 ± 0.008 km/s, and Poisson's ratio of 0.263 ± 0.008. All samples, base plates, and impactors were machined to the

TABLE I. Relevant measured and calculated experimental quantities including the projectile velocity, cerium Hugoniot data, and sounds speeds for F impact and T experiments.

Experiment	Impactor target material	V_p ±0.1% (km/s)	u_p (km/s)	U_s (km/s)	P_x (GPa)	Longitudinal sound speed (km/s)	Bulk sound speed (km/s)	Poisson ratio
(F)56-05-13[a]	Ce/LiF	0.473	0.384 ± 0.002	1.539 ± 0.027	3.99 ± 0.060			
(F)56-06-25[a]	Ce/LiF	0.496	0.307 ± 0.002	1.299 ± 0.022	2.70 ± 0.041			
(F)69-06-15[a]	Ce/LiF	0.921	0.509 ± 0.005	1.818 ± 0.032	6.26 ± 0.093	4.592 ± 0.100	3.295 ± 0.060	0.214 ± 0.011
(F)06-07-21	Ce/LiF	1.788	0.885 ± 0.010	2.579 ± 0.048	15.25 ± 0.23			
(F)56-08-11[b]	Ce/Sapp.	0.611	0.482 ± 0.002	1.800 ± 0.030	5.80 ± 0.087	4.523 ± 0.100	3.360 ± 0.060	0.247 ± 0.010
(F)69-09-04	Ce/LiF	1.123	0.598 ± 0.006	2.043 ± 0.036	8.170 ± 0.12	4.771 ± 0.109	3.726 ± 0.076	0.293 ± 0.016
(F)69-09-10	Ce/LiF	1.290	0.684 ± 0.007	2.100 ± 0.037	9.610 ± 0.14	4.571 ± 0.110	4.024 ± 0.115	0.398 ± 0.021
(F)69-09-13	Ce/LiF	1.417	0.730 ± 0.007	2.270 ± 0.041	11.08 ± 0.17	4.482 ± 0.118	4.347 ± 0.147	0.477 ± 0.025
(F)69-09-24	Ce/LiF	1.570	0.790 ± 0.008	2.429 ± 0.045	12.83 ± 0.17			
(F)69-09-30	Ce/LiF	1.497	0.752 ± 0.008	2.421 ± 0.045	12.17 ± 0.18	4.671 ± 0.086	4.505 ± 0.098	0.472 ± 0.011
(F)69-09-34	Ce/LiF	1.557	0.791 ± 0.008	2.377 ± 0.045	12.57 ± 0.19	4.676 ± 0.080	4.502 ± 0.084	0.471 ± 0.015
(F)1S-1421	Ce/LiF	1.247	0.453 ± 0.002	1.734 ± 0.022	5.25 ± 0.053			
(F)1S-1422	Ce/LiF	1.268	0.452 ± 0.002	1.743 ± 0.022	5.27 ± 0.053			
(F)1S-1424	Ce/LiF	1.260	0.452 ± 0.002	1.743 ± 0.022	5.27 ± 0.053			
(T)06-07-15	Cu/Cu-Ce-LiF	1.280	0.892 ± 0.005	2.632 ± 0.030	15.69 ± 0.12		5.080 ± 0.120	
(T)06-07-16	Cu/Cu-Ce-LiF	0.892	0.647 ± 0.005	2.175 ± 0.060	9.410 ± 0.19			
(T)06-07-19	Cu/Cu-Ce-LiF	1.119	0.794 ± 0.005	2.415 ± 0.020	12.83 ± 0.10		4.748 ± 0.085	
(T)06-07-18	Cu/Cu-Ce-LiF	1.158	0.819 ± 0.005	2.463 ± 0.040	13.48 ± 0.15		4.763 ± 0.155	
(T)56-04-15[a]	304SS/Ce-LiF	0.261	0.228 ± 0.001	0.955 ± 0.010	1.880 ± 0.03			
(T)06-07-25	Cu/Cu-Ce-LiF	1.425	0.985 ± 0.005	2.745 ± 0.028	18.08 ± 0.15		5.029 ± 0.150	
(T)56-09-24	Al/Al-Ce-LiF	0.333	0.219 ± 0.002	0.925 ± 0.005	1.683 ± 0.011			

[a]The ambient density for these cerium samples were 6.77 g/cc.
[b]This experiment used a sapphire optical window.

desired diameter and thickness then lapped flat and parallel within 3–5μm. Ultrapure LiF(100) crystals (Reflex Analytical) were used as optical windows for the PDV and VISAR diagnostics. These windows were optically polished on both sides, flat and parallel to 0.0002 inch, and oriented within ±15 min. The nominal window thickness was 19 mm and the ambient density for the LiF was 2.641 (g/cm^3).

III. EXPERIMENTAL RESULTS

Twenty-one experiments were performed on cerium in this work including 14 front-surface impact experiments and 7 transmission experiments (four experiments used multiple cerium samples). The relevant experimental parameters and measured quantities are shown in Table I. The projectile velocity (km/s), the impactor/target material, the particle velocity (km/s), shock velocity (km/s), and longitudinal stress (GPa) are shown in columns three through six, respectively. The measured sound speed (km/s) for the initial release wave through cerium is shown in column seven. For some of the experiments, it was possible to measure the velocity of the bulk wave during release. The sound speed for this wave is shown in column eight. Values for Poisson's ratio were calculated using the sound-speed values and the equation $\nu=(3C_B^2-C_L^2)/(3C_B^2+C_L^2)$, where C_B and C_L represent the bulk and longitudinal sounds speeds, respectively. The values for Poisson's ratio are shown in column nine.

Wave profiles from five of the front-surface impact experiments are shown in Fig. 3 where particle velocity (km/s) is plotted versus time (μs). The data show a sharp shock jump to a steady state followed by a release from the back of the impactor. A rarefaction shock is observed in the data during release likely due to crossing the low-pressure γ-α phase boundary. Such rarefaction shocks have been observed previously in iron when unloading across the α-ϵ phase boundary.[26]

The front-surface impact data were used to determine the sound speed at pressure. As shown in Fig. 4, the time duration of the peak state ΔT is bounded by the arrival of the initial shock jump (due to impact) and the arrival of the release wave (generated from the back of the cerium sample) at the cerium-LiF interface. This release wave propagates at the sound-velocity characteristic of the material at pressure and is related to the shock velocity U_s [obtained from Eq. (3)], the sample thickness x, and ΔT through the equation

$$C=\left[\frac{\Delta T}{x}-\frac{1}{U_S}\right]^{-1} \quad (1)$$

where ΔT is the time difference between the release arrival time (t_1) and the impact time (t_o). An example calculation is

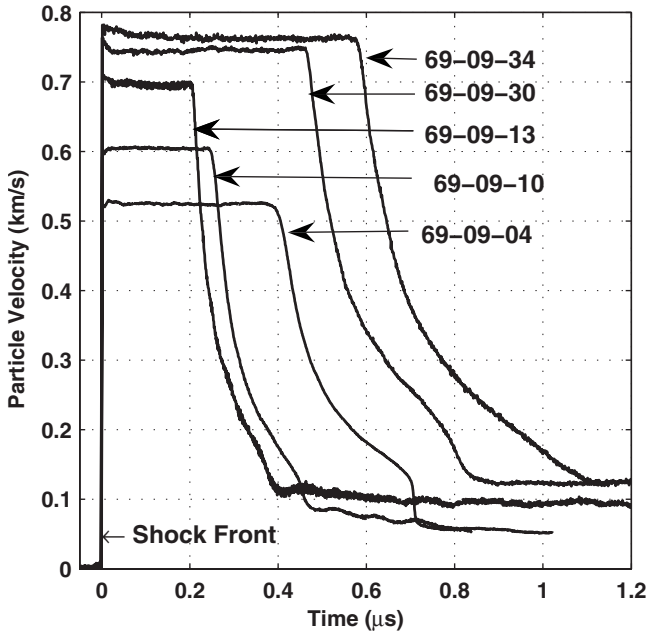

FIG. 3. Wave-profile data obtained from the front-surface impact experiments.

shown in Fig. 4 using the wave-profile data to determine the longitudinal and bulk sound speed for experiment 69-09-04. For the longitudinal wave speed, ΔT is the difference between the initial release arrival time (t_1) and impact (t_o). To determine the bulk wave speed, Eq. (1) was used to calculate

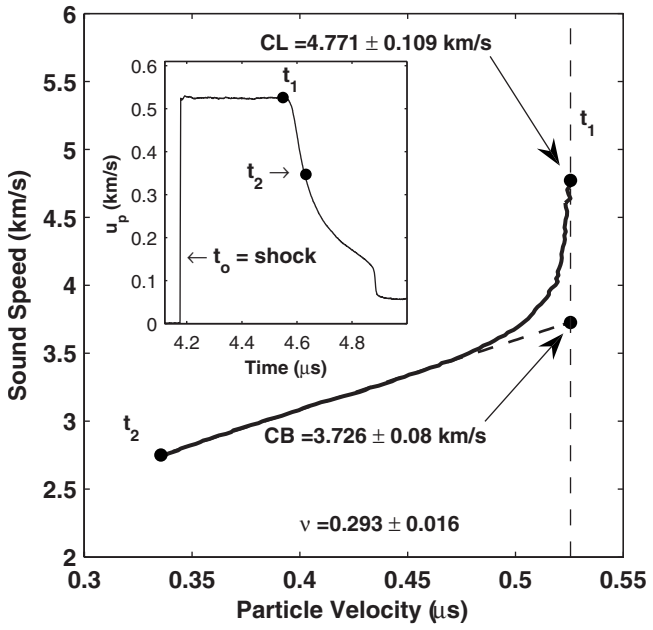

FIG. 4. Sound speed plotted versus particle velocity for the release portion of the wave profile for experiment 69-09-04. The vertical dashed line represents the peak particle velocity state. (inset) Wave-profile data used for the calculation that shows the relevant portion of the data (time is arbitrarily shifted with respect to impact). The sample thickness was 0.536 mm and the estimated arrival times corresponding to the events shown in the figure were t_o =4.1763 μs, t_1=4.5491 μs, and t_2=4.5803 μs.

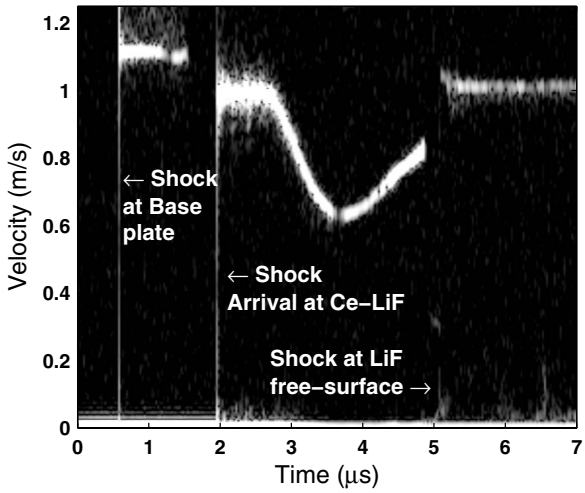

FIG. 5. Analyzed Doppler velocimetry data for experiment 06-07-19. The particle velocity (km/s) is plotted versus time (μs). Note that the window correction factor for 1550-nm laser light (Ref. 33) has not been applied to the data shown in Fig. 5.

the sound speed as a function of particle velocity during release where the value of t_1 ranged from the initial release to a second point t_2 further along the release. The linear portion of the release was fit with a line and the bulk sound speed was taken as the value corresponding to the peak particle velocity. The resulting values for the sound speed are shown in Table I (column seven and eight). Work is underway to obtain estimates of strength using the release data shown in Fig. 4.

An example of PDV data obtained from one of the transmission experiments is shown in Fig. 5 (shot 06-07-19) where particle velocity is plotted versus time. In this experiment, a copper impactor (3.908 mm) was accelerated to a velocity of 1.119 km/s to impact a copper base plate (3.915 mm) backed by a cerium sample (3.325 mm) and an LiF optical window. Three impact events are visible in the data including shock breakout at the baseplate free-surface (at 0.6 μs), shock arrival at the cerium-LiF interface (at 2 μs), and shock arrival and subsequent motion of the LiF-free surface (at 5 μs). Similar to the front-surface data, the wave profile at the cerium-LiF interface exhibits a shock jump to a peak state followed by release. For experiments where multiple samples were used, the release wave was observed to overtake the shock front as a function of sample thickness.

The VISAR wave profiles (for all four samples) corresponding to the PDV data shown in Fig. 5 are shown in Fig. 6. Similar to the PDV data (see Fig. 5) the wave profiles exhibit a shock jump to a steady state followed by a release. As expected, the time duration of the peak state was observed to decrease as the sample thickness increased because of overtake of the release wave with the shock front. These data were used to determine the sound speed using the standard overtake-method analysis discussed in detail elsewhere.[23,28] Briefly, the sample thickness x was plotted versus the corresponding peak state time duration (see Fig. 6 inset) to determine the overtake distance X_{max} defined as the thickness where the release overtakes the shock front (y intercept in the plot). Next, the measured shock velocity and

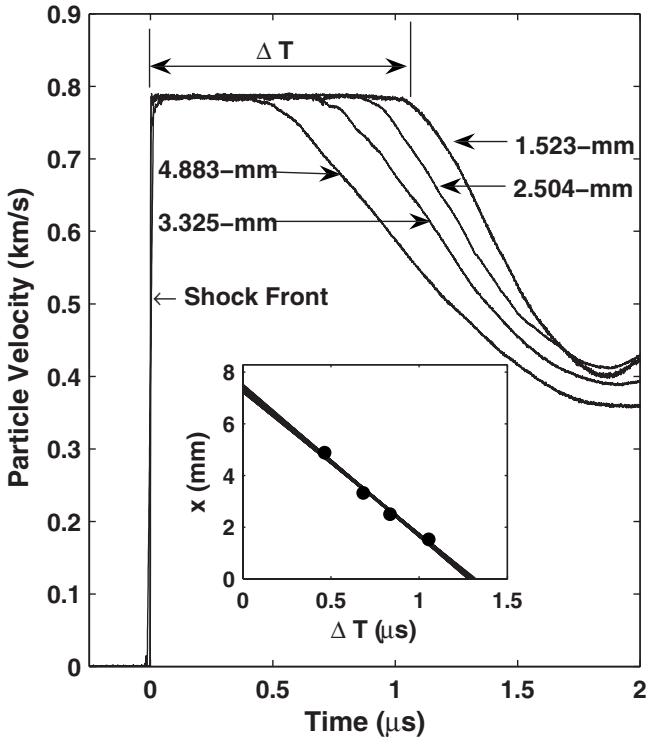

FIG. 6. Measured wave profiles for experiment 06-07-19. Particle velocity (km/s) is plotted versus time (μs) for four samples with varying thicknesses. A plot of the sample thickness x (mm) versus peak state time duration ΔT is shown in the inset figure. The values for ΔT were 1.0544 μs, 0.8348 μs, 0.6832 μs, and 0.4644 μs corresponding to increasing sample thickness.

the value for X_{max} were used to calculate the Lagrangian sound speed C using the equation

$$C = X_{max}\left[t_{SW} - t_{RW} + \frac{X_{max}}{U_s}\right]^{-1}, \tag{2}$$

where t_{SW} and t_{RW} are the shock wave and release wave arrival times at the front of the cerium sample, respectively. These values were obtained from a wave propagation code that incorporated the shock response of the baseplate and impactor. For experiment 06-07-19, the value for X_{max} was 7.367 mm and the calculated values for t_{SW} and t_{RW} were 0.8208 and 2.319 μs. Using Eq. (2), the sound speed was determined to be 4.748 km/s.

Uncertainty estimates were obtained for the sound-speed values by using a Monte Carlo approach to propagate the error in each measurement. For example, to calculate X_{max} from the data shown in Fig. 6 (inset), each data point was represented by a normal distribution where the center was taken as the measured value and the width (at 1-sigma) was assumed to be equal to the measurement uncertainty. Next, data points were randomly picked from each distribution and then a line was fit to this new data set using the standard least-squares method. The value for X_{max} was obtained for each line (value of x corresponding to $\Delta T=0$) which was then used to generate a histogram where the center was taken as the value for X_{max}. The distribution width (at 1-sigma) was taken as the estimated uncertainty. The solid lines shown in Fig. 6 (inset) were obtained using this method and represent all possible lines through the data. This methods extends easily to the other values recorded in Table I including those obtained from the front-surface impact experiments.

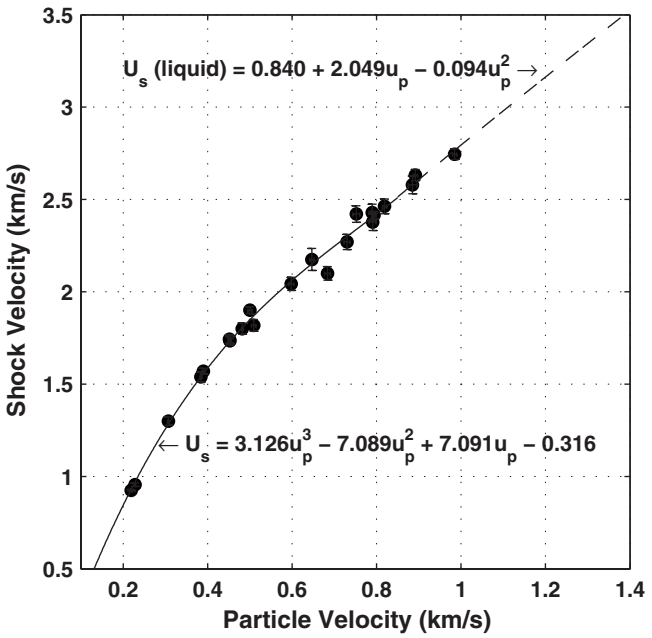

FIG. 7. Shock velocity (km/s) plotted as a function of the particle velocity (km/s) for all available low-pressure data. The solid curve is a fit to the data and the dashed line is the corresponding fit to the higher-pressure data (see Fig. 8). The uncertainty in the fit was estimated to be approximately 1% from 0.2 to 0.85 km/s.

IV. ANALYSIS AND DISCUSSION

A summary of all available Hugoniot data obtained in this work as well as past work[22,23] is shown in Fig. 7 and 8 where the shock velocity (km/s) is plotted versus the particle velocity (km/s). The shock response for the low-pressure regime (Fig. 7) is nonlinear and the data were best fit using a cubic polynomial given by the equation

$$U_s = 3.125u_p^3 - 7.089u_p^2 + 7.091u_p - 0.316, \tag{3}$$

which is valid between approximately 0.2 and 0.9 km/s (Table II). The higher-pressure data were best fit to a quadratic equation given by the equation $U_s=0.840+2.049u_p - 0.094u_p^2$ which is shown in Fig. 7 as the dashed line. The sound-speed data are also summarized in Fig. 8. A linear fit ($C_B=1.981+3.096u_p$) to the high-pressure sound speed data is also indicated in the figure.

For the low-pressure sound-speed data shown Fig. 8, the release wave exhibited a two-wave structure (also see Fig. 4) typical of an elastic-plastic response where the initial release wave travels at the longitudinal wave speed (C_L) followed by the slower plastic release wave (C_P). The plastic wave speed was fit to a line resulting in the equation $C_P=1.067 +4.489u_p$. For comparison with the data, this equation was used to calculate a longitudinal-wave speed function (dashed line) assuming constant value for Poisson's ratio ($\nu=0.263$).

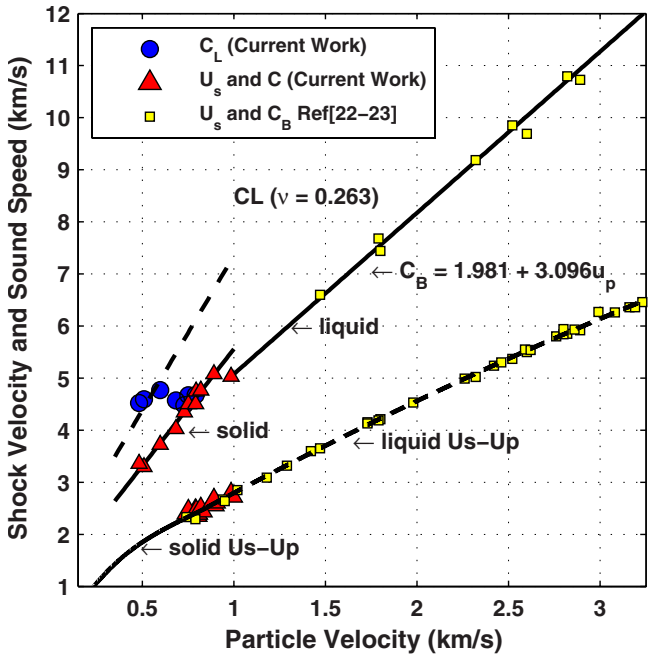

FIG. 8. (Color online) Sound-speed data (km/s) plotted as a function of the particle velocity (km/s) for all available experimental data. The U_s-u_p curves are also shown for comparison.

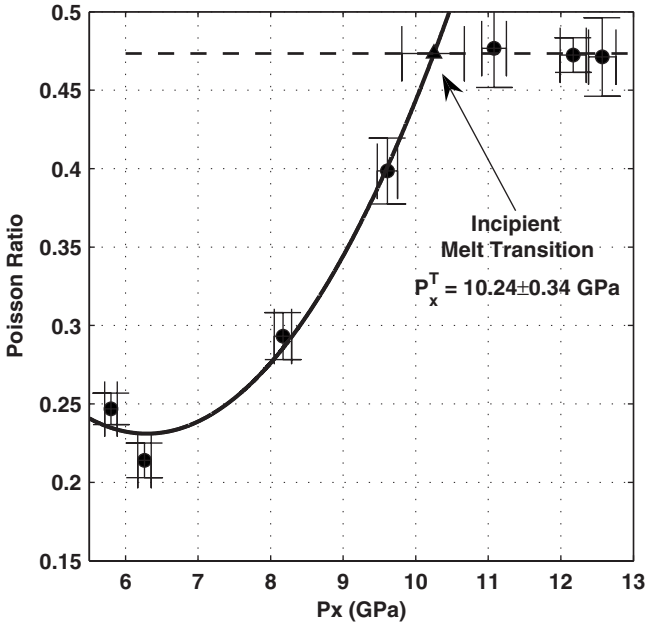

FIG. 9. Poisson ratio data versus the impact stress. The solid line is a quadratic fit using the first four low-pressure data points to estimate the incipient melt transition.

As the impact stress (or particle velocity) increases, the two wave speeds become coincident at approximately 10 GPa above which a single release wave is observed to propagate through the sample. This transition is interpreted as the onset of the melt transition. The transition stress was more accurately determined using the Poisson's ratio data shown in Fig. 9. The values for ν are observed to increase rapidly from the low-pressure value of 0.214 at 6.2 GPa to a value of approximately 0.48 at 11 GPa. The transition stress was determined by fitting the data to a quadratic function resulting in a transition stress of 10.24 ± 0.34 GPa corresponding to a shock velocity of 2.224 ± 0.027 km/s and a particle velocity of 0.687 ± 0.015 km/s. The sound-speed value obtained from experiment 06-07-25 is consistent with the liquid phase response likely indicating that the melt transition has completed by 18 GPa.

The behavior of ν as a function of the impact stress (as shown in Fig. 7) suggests that significant softening of the material occurs as the impact stress increases toward the melt transition. These results are similar to previous work on copper[5] (also an fcc structure) which showed significant softening up to incipient melt, observed as a gradual drop in sound speed, followed by a mixed phase region that extended over approximately 30 GPa to the pure liquid phase. The author's discuss possible explanations which include differential melting along the grain boundaries due to shock interaction with heterogeneities, inclusions, etc. Because of the lack of data available for cerium, additional work is required to fully examine the underlying mechanisms for the observed behavior which may include studies on phase-dependent strength.

In addition to Hugoniot and sound-speed data, two additional features were observed in the front-surface impact data shown in Fig. 3. The first feature is a transient spike in the particle velocity followed by a relaxation to lower values that is observed for impact stresses greater than 9.6 kbar (shot 69-09-10). This feature may be due to the solid-liquid transition where the relaxation rate represents the transition kinetics similar to previous work on iron.[26] However, as the impact stress increases from 11 to 13 GPa, the relaxation rate appears to decrease and then increase which is unexpected. Unlike iron samples, cerium samples readily form an oxide layer at the surface following sample preparation and may make transition kinetic measurements through front-surface impact experiments more difficult to perform consistently. The second feature is a rapid decrease in particle velocity observed during the release which is believed to be caused

TABLE II. Parameters for polynomial fits to data for the function $y = a_o + a_1 u_p + a_2 u_p^2 + a_3 u_p^3$.

Quantity	Approx. range (km/s)	a_o	a_1	a_2	a_3
U_s	$0.2 < u_p < 0.9$	−0.316	7.091	−7.089	3.125
U_s	$u_p > 0.9$	0.840	2.049	−0.094	
C_P	$0.2 < u_p < 0.9$	1.067	4.489		
C_B	$u_p > 0.9$	1.981	3.096		

by reversion from the α phase back to the γ phase. Recent calculations using a multiphase equation-of-state support this conclusion.[13] This feature is observed to become less pronounced as the impact stress increases and is not observed in experiment 69-09-34 where the impact stress is nearly 2 GPa above the melt transition. This may indicate that the material remains in the liquid state (or on the phase boundary) during release although additional work is required to verify this. Work is underway to use these data and a preheat capability to map the low-pressure γ-ϵ phase boundary. ‘

V. SUMMARY AND CONCLUSIONS

Shock-wave experiments were performed to examine the dynamic melt transition for cerium. Front-surface impact and transmission experiments were used to obtain Hugoniot data for the solid and liquid phases of cerium as well as sound speeds at pressure. A change in slope of the Hugoniot (U_s-u_p) pointed to a phase transition near 11 GPa but the similarity in the slope of the data spanning the discontinuity precluded a determination of the transition stress. In contrast, sound-speed data showed a more significant indicator of the melt transition. For the experiments with lower impact stresses, a structured release wave was observed which propagated at the longitudinal and plastic wave speeds. As the impact stress increased to values greater than 10 GPa, the difference between these two waves speeds was observed to decrease resulting in a single release wave propagating through the sample. At approximately 18 GPa, the sound speed was in agreement with high-pressure liquid sound-speed curve. These results lead to the conclusion that cerium begins to melt at 10.24 ± 0.34, as determined using the Poisson ratio data and likely remains in a mixed phase until approximately 18 GPa where the melt transition is complete.

The experiments and data analysis shown here provide important information regarding the shock-melting process for cerium including the stress for the onset of the melt transition that is required for validation of the multiphase equation of state[13] that includes the solid-liquid boundary. In addition to the melt transition, work is underway to obtain estimates of strength as a function of impact stress, to perform a more complete analysis of the rarefaction shock during release,[13] and preheat experiments to map γ-α phase boundary. Such experiments are expected to provide important information on the multiphase properties of cerium to further increase the knowledge and understanding of dynamic phase transitions and associated kinetics.

ACKNOWLEDGMENTS

This work was performed at Los Alamos National Laboratory operated by Los Alamos National Security, LLC for the U.S. Department of Energy’s NNSA under Contract No. DE-AC52-06NA25396. The high-pressure liquid data shown here is the result of an international collaboration between RFNC-VNIIEF and Los Alamos National Laboratory (LANL) under Contract No. 37713-000-02-35. Jim Esparza, Tim Piece, and Chuck Owens are gratefully acknowledged for their help in target and projectile fabrication, gun setup, and shot execution. Adam Iverson and Jason Young (NSTech) are thanked for their assistance with PDV probe setup for the multislug experiments.

*bjjensen@lanl.gov

[1] G. E. Duvall and R. A. Graham, Rev. Mod. Phys. **49**, 523 (1977).
[2] R. S. Hixson, D. A. Boness, J. W. Shaner, and J. A. Moriarty, Phys. Rev. Lett. **62**, 637 (1989).
[3] P. A. Urtiew and R. Grover, J. Appl. Phys. **48**, 1122 (1977).
[4] C. Dai, X. Jin, X. Zhou, J. Liu, and J. Hu, J. Phys. D **34**, 3064 (2001).
[5] D. Hayes, R. S. Hixson, and R. G. McQueen, in *Shock Compression of Condensed Matter*, edited by M. D. Furnish, L. C. Chhabilidas, and R. S. Hixson (American Institute of Physics, Melville, New York, 1999), pp. 483–488.
[6] J. H. Nguyen and N. C. Holmes, in *Shock Compression of Condensed Matter*, edited by M. D. Furnish, L. C. Chhabilidas, and R. S. Hixson (American Institute of Physics, Melville, New York, 2000), pp. 81–84.
[7] J. M. Brown, J. N. Fritz, and R. S. Hixson, J. Appl. Phys. **88**, 5496 (2000).
[8] J. M. Brown and R. G. McQueen, J. Geophys. Res. **91**, 7485 (1986).
[9] C. S. Yoo, N. C. Holmes, M. Ross, D. J. Webb, and C. Pike, Phys. Rev. Lett. **70**, 3931 (1993).
[10] I. L. Aptekar, V. I. Rashchupkin, and E. Yu. Tonkov, Sov. Phys. Solid State **24** (8), 1432 (1982).
[11] B. L. Davis and L. H. Adams, J. Phys. Chem. Solids **25**, 379 (1964).
[12] G. Eliashberg and H. Capellmann, JETP Lett. **67**, 125 (1998).
[13] F. J. Cherne, B. J. Jensen, and V. M. Elkin, in *Shock Compression of Condensed Matter-2009*, edited by M. Elert, W. T. Buttler, M. D. Furnish, W. W. Anderson, and W. G. Proud (American Institute of Physics, Melville, New York, 2009), pp. 1161–1164.
[14] S. Endo, H. Sasaki, and T. Mitsui, J. Phys. Soc. Jpn. **42**, 882 (1977).
[15] Ph. Schaufelberger, J. Appl. Phys. **47**, 2364 (1976).
[16] E. King, J. A. Lee, I. R. Harris, and T. F. Smith, Phys. Rev. B **1**, 1380 (1970).
[17] B. Sitaud, J. Pere, and Th. Thevenin, High Press. Res. **12** (3), 175 (1994).
[18] A. Jayaraman, Phys. Rev. **137**, A179 (1965).
[19] B. J. Jensen, in *Shock Compression of Condensed Matter-2009*, edited by M. Elert, W. T. Buttler, M. D. Furnish, W. W. Anderson, and W. G. Proud (American Institute of Physics, Melville, New York, 2009), pp. 1165–1170.
[20] A. K. Singh, High Temp. - High Press. **12**, 47 (1980).
[21] M. N. Pavlovskii, V. V. Komissarov, and A. R. Kutsar, Combust., Explos. Shock Waves **35**, 88 (1999).
[22] W. J. Carter, J. N. Fritz, S. P. Marsh, and R. G. McQueen, J.

Phys. Chem. Solids **36**, 741 (1975).
[23] M. V. Zhernokletov, A. E. Kovalev, V. V. Komissarov, M. G. Novikov, M. A. Zocher, and F. J. Cherne, in *Shock Compression of Condensed Matter*, edited by M. Elert, M. D. Furnish, R. Chau, N. Holmes, and J. Nguyen (American Institute of Physics, Melville, New York, 2007), pp. 117–120.
[24] V. M. El'kin, E. A. Kozlov, E. V. Kakshina, and Yu. S. Moreva, Phys. Met. Metallogr. **101**, 208 (2006).
[25] L. M. Barker and R. E. Hollenbach, J. Appl. Phys. **45**, 4872 (1974).
[26] B. J. Jensen, G. T. Gray III, and R. S. Hixson, J. Appl. Phys. **105**, 103502 (2009).
[27] R. G. McQueen, J. W. Hopson, and J. N. Fritz, Rev. Sci. Instrum. **53**, 245 (1982).
[28] J. N. Fritz, in *Shock Compression of Condensed Matter*, edited by M. D. Furnish, L. C. Chhabilidas, and R. S. Hixson (American Institute of Physics, Melville, New York, 1999), pp. 239–244.
[29] D. B. Hayes, J. Appl. Phys. **45**, 1208 (1974).
[30] B. J. Jensen, Los Alamos National Laboratory Report No. LA-14386, 2009 (unpublished).
[31] B. J. Jensen and J. Esparza, in *Shock Compression of Condensed Matter-2009*, edited by M. Elert, W. T. Buttler, M. D. Furnish, W. W. Anderson, and W. G. Proud (American Institute of Physics, Melville, New York, 2009), pp. 685–688.
[32] W. F. Hemsing, Rev. Sci. Instrum. **50**, 73 (1979).
[33] B. J. Jensen, D. B. Holtkamp, P. A. Rigg, and D. H. Dolan, J. Appl. Phys. **101**, 013523 (2007).
[34] A. C. Mitchell and W. J. Nellis, J. Appl. Phys. **52**, 3363 (1981).
[35] R. Feng and Y. M. Gupta, Shock Dynamics Center Technical Report No. 96-XX, 1994 (unpublished).
[36] R. G. McQueen, S. P. Marsh, J. W. Taylor, J. N. Fritz, and W. J. Carter, in *High Velocity Impact Phenomena*, edited by R. Kinslow (Academic Press, New York, 1970), pp. 293–417.
[37] F. J. Cherne, P. A. Rigg, W. W. Anderson, and J. C. Cooley, in *Shock Compression of Condensed Matter-2007*, edited by M. Elert, M. D. Furnish, R. Chau, N. Holmes, and J. Nguyen (American Institute of Physics, Melville, New York, 2006), pp. 489–492.